View metadata, citation and similar papers at core.ac.uk

brought to you by CORE

provided by Edinburgh Research Explorer

THE UNIVERSITY of EDINBURGH

Edinburgh Research Explorer

Potential origins of 400-500 kyr periodicities in the ocean carbon cycle: A box model approach

Citation for published version:
Russon, T, Paillard, D & Elliot, M 2010, 'Potential origins of 400-500 kyr periodicities in the ocean carbon cycle: A box model approach' Global Biogeochemical Cycles, vol. 24, no. 2, GB2013, pp. 1-16. DOI: 10.1029/2009GB003586

Digital Object Identifier (DOI):
10.1029/2009GB003586

Link:
Link to publication record in Edinburgh Research Explorer

Document Version:
Publisher's PDF, also known as Version of record

Published In:
Global Biogeochemical Cycles

Publisher Rights Statement:
Published in Global Biogeochemical Cycles by the American Geophysical Union (2010)

General rights
Copyright for the publications made accessible via the Edinburgh Research Explorer is retained by the author(s) and / or other copyright owners and it is a condition of accessing these publications that users recognise and abide by the legal requirements associated with these rights.

Take down policy
The University of Edinburgh has made every reasonable effort to ensure that Edinburgh Research Explorer content complies with UK legislation. If you believe that the public display of this file breaches copyright please contact openaccess@ed.ac.uk providing details, and we will remove access to the work immediately and investigate your claim.

Download date: 05. Apr. 2019

Click Here for Full Article

Potential origins of 400–500 kyr periodicities in the ocean carbon cycle: A box model approach

T. Russon,[1,2] D. Paillard,[1] and M. Elliot[2]

Received 27 May 2009; revised 10 November 2009; accepted 11 February 2010; published 28 May 2010.

[1] Cenozoic proxy records of both the isotopic composition of dissolved inorganic carbon in the oceans ($\delta^{13}C_{DIC}$) and deep ocean carbonate preservation show significant periodicities in the range 400–500 kyr. Sensitivity analysis of the ocean carbon cycle to potential variability on this timescale in patterns of global oceanic primary productivity and/or continental weathering fluxes is performed using a 7 box ocean-atmosphere model. The data constraints imposed by Plio-Pleistocene proxy records of $\delta^{13}C_{DIC}$, carbonate preservation, and atmospheric pCO_2 variability allow different scenarios to be evaluated. Forcing with the global oceanic primary production ratio of inorganic and organic carbon leads to the relative phases of response most consistent with the proxy data. However, only when changes also occur in total marine primary production can the observed relative amplitudes of $\delta^{13}C_{DIC}$ and pCO_2 variability also be reproduced. This scenario is consistent with oscillations between a highly productive, coccolithophore-rich global ocean and a less productive, diatom-rich one. Such oscillations have been proposed to originate from the orbital eccentricity cycle leading to changes in seasonality and thus silica utilization in the Southern Ocean. However, the period of response in model $\delta^{13}C_{DIC}$ is always close to that of the forcing function used, and thus a significant discrepancy remains between the orbital eccentricity cycle period of 413 kyr and the observed ~500 kyr $\delta^{13}C_{DIC}$ periodicity seen in the Pleistocene.

Citation: Russon, T., D. Paillard, and M. Elliot (2010), Potential origins of 400–500 kyr periodicities in the ocean carbon cycle: A box model approach, *Global Biogeochem. Cycles*, *24*, GB2013, doi:10.1029/2009GB003586.

1. Introduction

[2] The study of paleoceanographic proxies in Cenozoic sediment core records has revealed the existence within the ocean-climate system of periodic variability longer than the characteristic glacial-interglacial cycles of 10–100 kyr [*Bickert et al.*, 1993; *Herbert*, 1997; *Imbrie et al.*, 1992, 1993; *Keigwin and Boyle*, 1985; *Raymo et al.*, 1997, 2006; *Wang et al.*, 2004]. Perhaps the most widely recognized such periodicity occurs in the carbon isotopic composition of foraminiferal calcite ($\delta^{13}C_{calcite}$), a proxy for the isotopic composition of the dissolved inorganic carbon (DIC) in the surrounding seawater ($\delta^{13}C_{DIC}$). Strong periodicities in the range 400–500 kyr are present in Plio-Pleistocene planktic and benthic $\delta^{13}C_{calcite}$ records from every major ocean basin [*Bickert et al.*, 1993; *Mix et al.*, 1995b; *Tiedemann et al.*, 1994; *Venz and Hodell*, 2002; *Wang et al.*, 2004]. Miocene [*Woodruff and Savin*, 1991] and Oligocene [*Palike et al.*, 2006] $\delta^{13}C_{calcite}$ records have been shown to also contain a significant ~400 kyr periodicity suggesting that some form of 400–500 kyr $\delta^{13}C_{DIC}$ cycles persist across at least the past 35 Myr. Such periodicities are not unique to $\delta^{13}C_{DIC}$ and records of sedimentary carbonate content, which relates to deep ocean carbonate preservation, from both the Miocene [*Moore et al.*, 1982] and Cretaceous [*Herbert et al.*, 1986] also show ~400 kyr cycles.

[3] Statistically robust identification of individual periodicities in the 400–500 kyr range within Plio-Pleistocene proxy records is often difficult due to the relatively large cycle and record duration ratio. However, high-resolution $\delta^{13}C_{calcite}$ records do yield significant results and the 5 Myr duration ODP Site 1143 benthic $\delta^{13}C_{calcite}$ record from the South China Sea is reproduced here [*Tian et al.*, 2002, 2006; *Wang et al.*, 2003, 2004] (Figure 1). The dominant > 100 kyr period in the record evolves from ~413 kyr in the Pliocene to ~500 kyr in the Pleistocene with spectral analysis of the whole record showing an averaged peak at 468 ka [*Wang et al.*, 2004] (Figure 1c). In lower resolution or shorter records, observation in the time domain, with all periods < 350 kyr removed, allows identification of potential 400–500 kyr "cycles." Applying this treatment to an Indian Ocean composite Grain Size Index (GSI) record, another proxy for carbonate preservation, shows a series of ~500 kyr "cycles" over the past 1.5 Myr [*Bassinot et al.*, 1994] (Figure 2). The record of atmospheric pCO_2 over the past 0.8 Myr from a composite of Antarctic ice core records [*Lüthi et al.*, 2008;

[1]LSCE, IPSL, Laboratoire Mixte CEA, CNRS, UVSQ, Gif-sur-Yvette, France.
[2]School of GeoSciences, University of Edinburgh, Edinburgh, UK.

Copyright 2010 by the American Geophysical Union.
0886-6236/10/2009GB003586

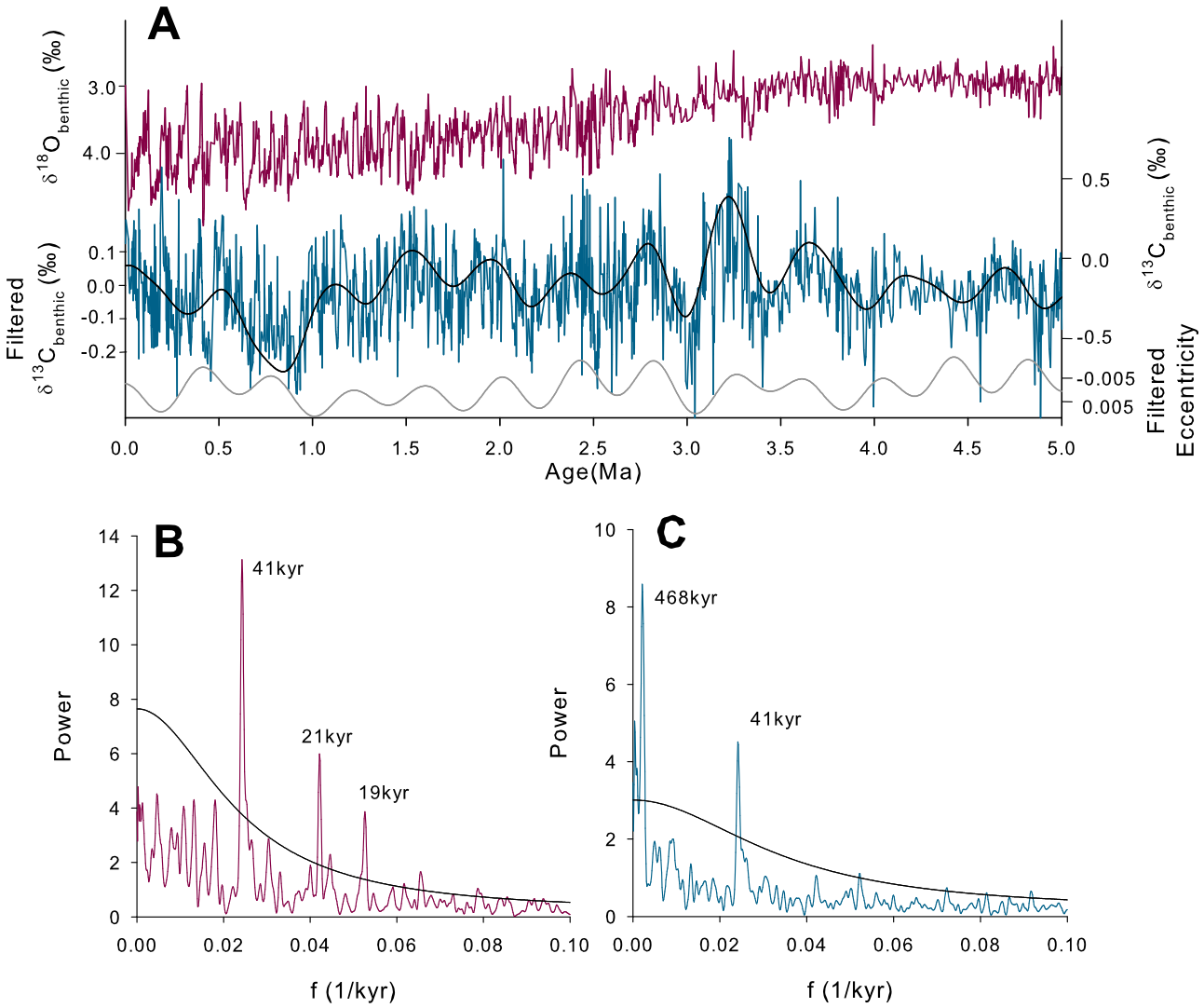

Figure 1. (a) ODP Site 1143 $\delta^{18}O_{benthic}$ and $\delta^{13}C_{benthic}$ data [*Wang et al.*, 2004] across the past 5 Myr: black line shows the $\delta^{13}C_{benthic}$ data after Gaussian filtering around 0 kyr^{-1} using a 0.0029 kyr^{-1} bandwith filter (removing all < 350 kyr periods), and gray line shows orbital eccentricity data filtered in the same way; (b) power spectra of ODP Site 1143 $\delta^{18}O_{benthic}$; and (c) $\delta^{13}C_{benthic}$ with 95% false alarm shown as black line. Spectral analysis performed on REDFIT software [*Schulz and Mudelsee*, 2002].

Petit et al., 1999] is dominated by ~100 kyr glacial and interglacial variability but also shows a single > 350 kyr "cycle" with a maxima at ~0.4 Ma (Figure 2). It therefore appears that some component of 400–500 kyr variability is present in most aspects of the global carbon cycle over the late Mesozoic and Cenozoic. Prior to the Pleistocene the dominant period seen in most records is consistently 400–413 kyr, but both the $\delta^{13}C_{DIC}$ and carbonate preservation cycles appear to "stretch" toward ~500 kyr over the past 2 Myr.

[4] Within the Pleistocene, major shifts in the mode of glacial-interglacial behavior have been proposed to be preceded by, or associated with, maxima in the ~500 kyr $\delta^{13}C_{DIC}$ cycle [*Wang et al.*, 2003, 2004]. The last major such shift occurred with the emergence of the dominant ~100 kyr glacial cycles during the Middle Pleistocene Transition (0.5–1.2 Ma) [*Head and Gibbard*, 2005] (Figure 2). Modeling studies suggest this transition may also constitute a fundamental change in the relationship between climatic and carbon cycle variables [*Kohler and Bintanja*, 2008]. The transition coincides with a significant negative excursion in mean ocean $\delta^{13}C_{DIC}$ that may constitute a ~500 kyr cycle minima [*Wang et al.*, 2004] or a one-off perturbation related uniquely to the climatic transition itself [*Hoogakker et al.*, 2006; *Raymo et al.*, 1997].

[5] The 400–500 kyr periodicities seen in carbon cycle proxies are not so clearly manifested in records of past climatic variability [*Herbert*, 1997; *Rial*, 2004]. The Oligocene ODP Site 846 $\delta^{18}O_{benthic}$ record, a proxy for global ice volume and deep water temperature, does show significant variance at ~405 kyr [*Palike et al.*, 2006]. However, the persistence of the 400–500 kyr carbon cycle peri-

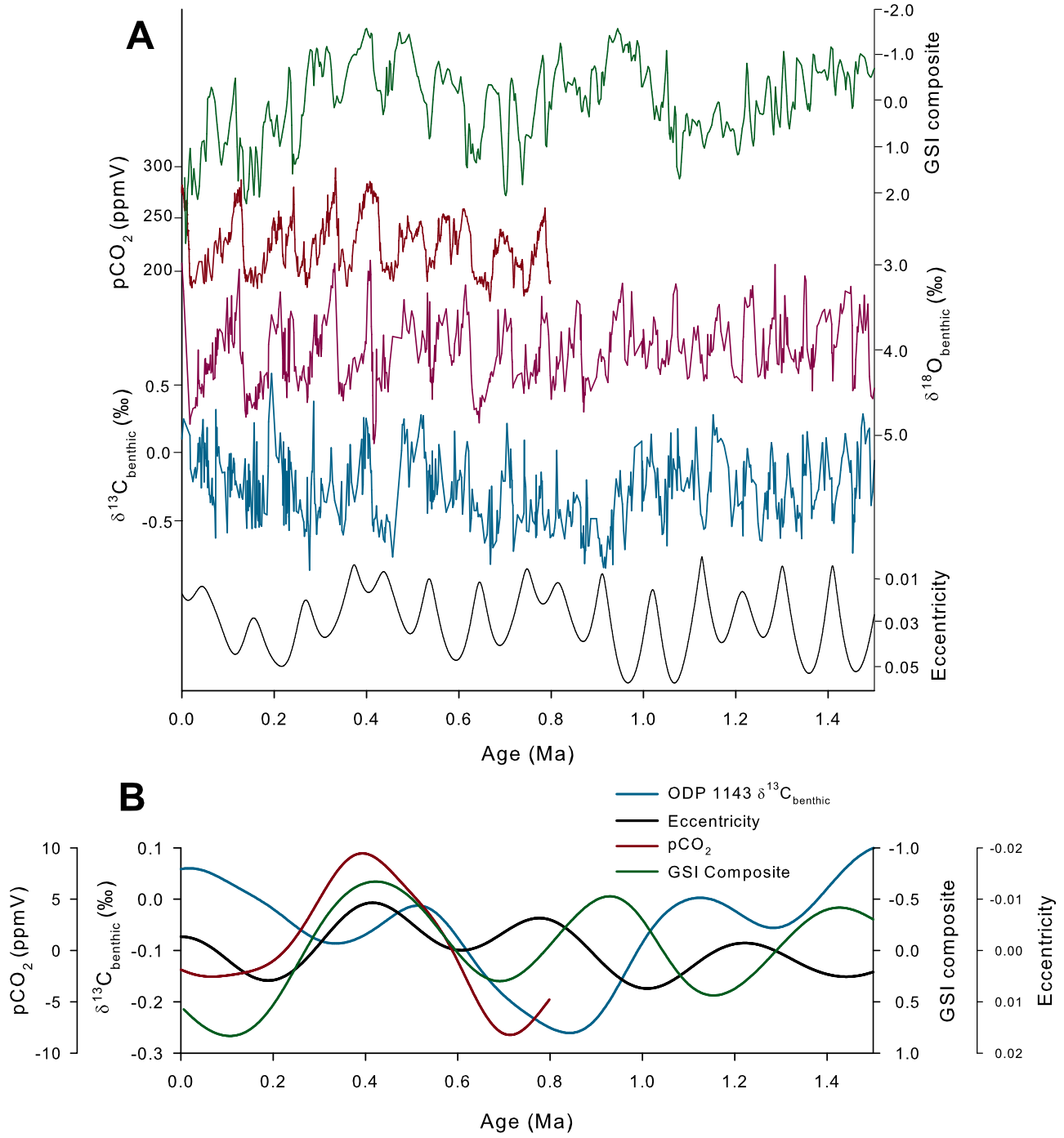

Figure 2. (a) GSI composite [*Bassinot et al.*, 1994], composite Antarctica pCO_2 record [*EPICA Community Members*, 2004], ODP Site 1143 $\delta^{18}O_{benthic}$ and $\delta^{13}C_{benthic}$ [*Wang et al.*, 2004], and orbital eccentricity [*Berger and Loutre*, 1991] over the past 1.5 Myr. (b) Gaussian filtering around 0 kyr^{-1} using a 0.0029 kyr^{-1} bandwith filter (removing all periods < 350 kyr) of the ODP Site 1143 $\delta^{13}C_{benthic}$, Antarctica composite pCO_2, GSI composite, and eccentricity data over the past 1.5 Myr.

odicities into the ice-free world of the Cretaceous [*Herbert et al.*, 1986; *Herbert*, 1997] suggests that the processes driving the cycles are not directly related to fluctuations in ice volume. No significant periodicity in the 400–500 kyr range is present in the ODP 1143 $\delta^{18}O_{benthic}$ record over the past 5 Myr [*Wang et al.*, 2004] (Figure 1b).

[6] Understanding the origin of the observed 400–500 kyr carbon cycle periodicities is an important first step toward elucidating the apparently complex and evolving relation-

ship between the carbon cycle and climate on these timescales. The orbital eccentricity cycle modulation of the precession cycle has a period of 413 kyr [*Berger and Loutre*, 1991] and is the most obvious external origin for the observed variability. Previous modeling studies have demonstrated that the carbon cycle tends to amplify long period components of the orbital forcing [*Palike et al.*, 2006], potentially explaining the relatively large response to a relatively weak 413 kyr orbital forcing. The orbital variations could potentially influence the carbon cycle through either changes in midlatitude and high-latitude seasonality and hence primary production regimes or through the global hydrological cycle leading to variability in the weathering fluxes of productivity-limiting nutrients, DIC and Alkalinity (ALK) into the global ocean. The present study does not investigate the direct influence of insolation variations but evaluates, using a simple ocean-atmosphere box model, whether these potential response mechanisms within the carbon cycle could produce the variability observed in the proxy records.

[7] The 400–500 kyr timescale of interest here falls between the geological (>1 Myr) and glacial-interglacial (10–100 kyr) timescales and is close to the residence time of DIC in the oceans [*Berner and Berner*, 1987]. On the geological timescale the global mean surface temperature is primarily controlled by the level of atmospheric pCO_2, determined in turn by the balance between volcanic and metamorphic degassing of carbon into the atmosphere and its removal through the weathering of silicate rocks [*Berner et al.*, 1983; *Li et al.*, 2009; *Raymo and Ruddiman*, 1992]. This weathered inorganic carbon reaches the ocean and ultimately forms new carbonate sediments. These processes are sufficiently slow however that on glacial-interglacial timescales the coupled ocean-atmosphere system behaves almost as a "closed" system with respect to DIC and ALK [*Archer et al.*, 2000]. Glacial-interglacial variability in atmospheric pCO_2 is thought to be caused by either the transfer of DIC to/from different parts of the closed system or through changes in the organic carbon (C_{org}) cycle [*Archer and Maier-Reimer*, 1994; *Archer et al.*, 2000; *Imbrie et al.*, 1993; *Sigman and Boyle*, 2000]. The C_{org} cycle may not be considered closed on even the glacial-interglacial timescale as the size of the terrestrial biosphere is dynamic, leading to changes in both mean ocean $\delta^{13}C_{DIC}$ and pCO_2 [*Crowley*, 1995; *Shackleton*, 1977]. It is thus possible that both open and closed system variability in both the inorganic and organic carbon cycles may play a role in the observed 400–500 kyr cycles and the model presented here includes first-order treatments of these processes.

[8] Numerical reconstructions on the Cenozoic timescale of global riverine fluxes of weathered inorganic carbon, ALK and productivity limiting nutrients are at present limited. Therefore, the approach taken here is to evaluate a wide range of forcing function amplitudes as a first attempt to constrain likely system sensitivity to each forcing. The effect on model output of the parameters used to define the box model itself is also considered. Finally, to evaluate the various scenarios, model output for deep ocean $\delta^{13}C_{DIC}$ (hereafter "$\delta^{13}C_{DIC}$") mean ocean carbonate ion concentration ($[CO_3^{-2}]_{mean}$, a proxy for carbonate preservation), and atmospheric pCO_2 is compared to available proxy data over the past 5 Myr. This period is selected, rather than a longer interval further back in time, due to the availability of multiple proxy constraints in the same interval allowing the evaluation of the relative phases of the variables as well as their periods and amplitudes. Three constraints are evaluated from this data comparison: (1) the amplitudes of periodic variability in $\delta^{13}C_{DIC}$ and pCO_2 (carbonate preservation output cannot be quantitatively compared to the proxy data); (2) the observed period of variability in $\delta^{13}C_{DIC}$, pCO_2 and carbonate preservation; and (3) the relative phases of the response in $\delta^{13}C_{DIC}$, pCO_2 and carbonate preservation.

2. Model Description

[9] Ocean-atmosphere box models simplify the complex 3-D dynamics of the global ocean and atmosphere into a series of finite "boxes" between which certain quantities, such as heat, or DIC, are advected. Such models possess the significant advantage of being able to simulate millions of years in a matter of minutes using a standard desktop computer. Many studies exist using box models to investigate first-order processes in the oceanic carbon cycle on glacial-interglacial [*Michel et al.*, 1995; *Toggweiler*, 1999, 2008] and longer timescales [*Hoogakker et al.*, 2006; *Palike et al.*, 2006]. The present study adapts the C++ box modeling tool BoxKIT [*Paillard*, 1995] to the study of the 400–500 kyr cycles through the incorporation of key open system processes in both the inorganic and organic carbon cycles. The closed system model used to represent the ocean-atmosphere system is based closely on that of an existing 7 box ocean model [*Toggweiler*, 1999] (Figure 3).

[10] Closed system box models on the glacial-interglacial timescale are able to reproduce to the first order several key features of climate on this timescale [*Toggweiler*, 1999]. However, the open system carbon cycle processes relevant to the longer timescales of interest here are relatively poorly understood in comparison to the closed system ones and only first-order parameterizations are appropriate. In the case of the DIC and ALK cycles, the present study closely follows the approach of *Toggweiler* [2008]. However, in order to develop a plausible treatment of $\delta^{13}C_{DIC}$ it is essential to also include some treatment of the organic carbon cycle on the same timescale. This is achieved by parameterizing the sedimentation of C_{org} as a function of primary productivity in the surface boxes such that model $\delta^{13}C_{DIC}$ remains within the bounds implied by $\delta^{13}C_{benthic}$ records over the past 5 Myr.

[11] The governing equations for each ocean box of the model may be summarized as

$$V_i \frac{dX_i}{dt} = \sum_j A_{ij} + \sum_j P_{ij} + \sum F \qquad (1)$$

Where V is the volume of box i, X is a model variable, A are the advected terms and P are the remineralization terms (Figure 3). The advection and remineralization regimes are defined as by *Toggweiler* [2008]. F are the various open system fluxes, as defined in sections 2.1 and 2.2. Not all combinations of boxes and variables require all terms to be

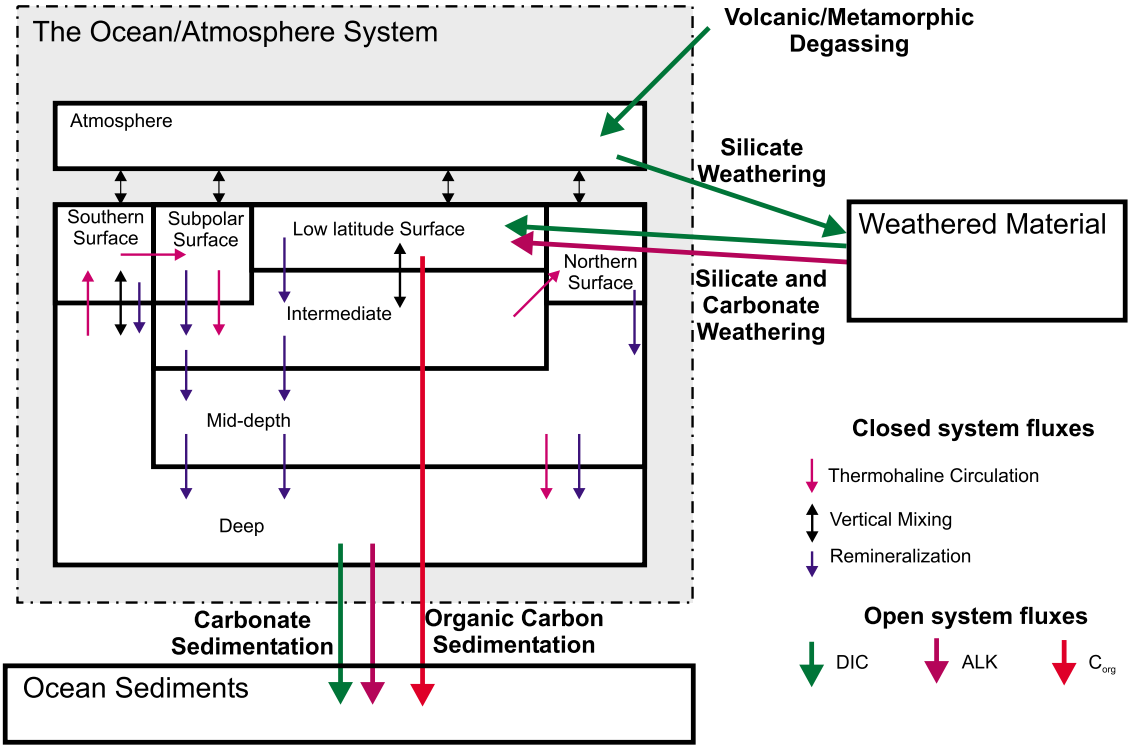

Figure 3. Schematic diagram of the 7 box ocean-atmosphere model and the additional open system fluxes (bold type) used in the present study. The 7 box model is based closely on that of *Toggweiler* [2008]. The dashed gray box represents the "closed" ocean-atmosphere system.

included. For example, in the case of the concentration of DIC in the low-latitude surface box the governing equation reduces to

$$V_L \frac{d[DIC]_L}{dt} = M_{LI}([DIC]_I - [DIC]_L) + FWEATH^{DIC} \quad (2)$$

The calculation of the $\delta^{13}C_{DIC}$ terms and the atmospheric parameters, such as pCO_2, is somewhat more complex and is explained in Appendix A.

2.1. Open System Processes: Inorganic Carbon and Alkalinity

2.1.1. Volcanic-Metamorphic Input of Carbon

[12] The principle external source of inorganic carbon to the ocean-atmosphere system on the timescales of interest is from the volcanic and metamorphic outgassing of CO_2. Parameterization of this flux is achieved through the addition of a fixed input of 160,000 mol C s^{-1} of DIC [*Marty and Tolstikhin*, 1998] directly to the surface ocean box. While this flux should strictly speaking enter the atmosphere, the mixing time between the atmosphere and surface ocean is sufficiently short compared to the other model processes that it can be neglected.

2.1.2. Continental Weathering of DIC and ALK

[13] On geological timescales the rate of weathering of continental silicate rocks (equation (3)) is thought to be a function of mean surface temperature and therefore the baseline level of atmospheric pCO_2 [*Berner et al.*, 1983; *Walker et al.*, 1981]. The riverine fluxes of weathered DIC and ALK (equations (4) and (5)) arising from silicate weathering are therefore parameterized as a linear function of pCO_2 [*Walker et al.*, 1981].

$$CaSiO_3 + 2CO_2 + 2H_2O \rightarrow 2HCO_3^- + 2H^+ + Ca^{2+} + SiO_3^{2-} \quad (3)$$

$$FSIL^{DIC} = k_{sil} + (1/\tau_{sil})pCO_2 \quad (4)$$

$$FSIL^{ALK} = 2(k_{sil} + (1/\tau_{sil})pCO_2) \quad (5)$$

For each mole of DIC added to the global ocean through silicate weathering, one mole of inorganic carbon is correspondingly removed from the atmospheric box (equation (3)). Thus, silicate weathering leads to the net transfer of ALK but not DIC into the ocean-atmosphere system. This leads to an increase in oceanic carbonate sedimentation which acts to remove both ALK and DIC from the system [*Berner et al.*, 1983]. At equilibrium, the net loss of DIC from this process balances the volcanic-metamorphic degassing flux.

[14] The values of the constants k_{sil} and τ_{sil} are taken as 62,300 mol C s^{-1} and 0.012 s ppmV mol C^{-1}, respectively, after *Toggweiler* [2008]. This equates to a $1/e$ folding time for the weathering feedback of 500 kyr and on timescales exceeding this, the atmospheric pCO_2 returns to a fixed

equilibrium value. Antarctic pCO_2 records show a decrease in mean value of up to 22 ppmV over the past 0.61 Myr, suggesting that while the system is indeed closely buffered by pCO_2, small imbalances in the open system fluxes do exist on this timescale [*Zeebe and Caldeira*, 2008]. Such a secular decrease in mean pCO_2 may be represented in the model using a linear variation in the k_{sil} term.

[15] The weathering of continental carbonate rocks (equation (6)) also depends on global surface temperature and is parameterized similarly to the silicate process (equations (7) and (8)) but without the fixed component terms [*Toggweiler*, 2008].

$$CaCO_3 + CO_2 + H_2O \rightarrow 2HCO_3^- + Ca^{2+} \quad (6)$$

$$FCARB^{DIC} = (1/\tau_{carb})pCO_2 \quad (7)$$

$$FCARB^{ALK} = (2/\tau_{carb})pCO_2 \quad (8)$$

In contrast to silicate weathering, carbonate weathering leads to the net transfer of ALK and DIC to the ocean-atmosphere system in the same ratio (2:1) as it will be eventually removed during carbonate sedimentation. As such, on timescales exceeding that of the carbonate compensation feedback, carbonate weathering has no effect on the feedback between pCO_2 and weathering.

[16] The fluxes of weathered DIC and ALK arising from equations (4) and (7) (for DIC) and (5) and (8) (for ALK) are added directly to the low-latitude surface ocean box. The value of the constant τ_{carb} is taken as 0.0030 s ppmV mol C^{-1} after *Toggweiler* [2008].

2.1.3. Carbonate Sedimentation

[17] Carbonate sedimentation leads to the loss of ALK and DIC from the deep ocean in the ratio 2:1 [*Marchitto et al.*, 2005]. Observations suggest that the mean oceanic Calcite Compensation Depth (CCD) does not undergo depth fluctuations greater than ± 250m from the modern depth (~4000m) anywhere in the Neogene [*Rea and Leinen*, 1985]. This implies that deep ocean carbonate ion concentrations ($[CO_3^{-2}]$) are tightly buffered around a long-term equilibrium value [*Zeebe and Westbroek*, 2003]. While the formation and dissolution of sedimentary $CaCO_3$ in the oceans are extremely complex processes, on the timescales of interest here a simple parameterization based on the deviation of $[CO_3^{-2}]$ from the long-term equilibrium value is appropriate (equations (9) and (10)) [*Toggweiler*, 2008].

$$FSED^{DIC} = (1/\tau_{sed})([CO_3^{-2}]_{deep} - [CO_3^{-2}]_{target}) \quad (9)$$

$$FSED^{ALK} = (2/\tau_{sed})([CO_3^{-2}]_{deep} - [CO_3^{-2}]_{target}) \quad (10)$$

All calcite sedimentation and dissolution is assumed to occur from/to the deep ocean box. Pelagic (as opposed to neritic) $CaCO_3$ production may constitute up to 85% of the modern global total [*Zeebe and Westbroek*, 2003] and thus the model does not include shelf sedimentation of carbonates. This may still be a significant omission, however and should be explored in future work. The $[CO_3^{-2}]_{target}$ value is set as 85 μmol L^{-1} and the $1/e$ folding time for this process is set, through τ_{sed}, at 5 kyr after *Toggweiler* [2008]. This parameterization means that fluctuations in model lysocline depth (which is assumed to relate directly to the CCD) are always less than ± 100m. If the feedback was relaxed such that larger fluctuations of up to ± 500m could occur, τ_{sed} would need to be ~30 kyr and the model lysocline becomes unacceptably deep. Such changes would not, however, significantly affect the amplitude, period or phase of the periodic response in $\delta^{13}C_{DIC}$ or pCO_2.

2.2. Organic Carbon Cycle Processes

[18] The silicate weathering and carbonate compensation feedbacks alone ensure that the DIC and ALK systems will always return to an equilibrium state. At this equilibrium, $[CO_3^{-2}]_{deep}$ will exceed $[CO_3^{-2}]_{target}$ by an amount sufficient for the net output of DIC to balance the long-term input from the volcanic-metamorphic degassing flux [*Toggweiler*, 2008]. This is not, however, the case for the $\delta^{13}C_{DIC}$ system as the $\delta^{13}C$ composition of the volcanic input flux is taken as being fixed at −5.0‰ [*Kump and Arthur*, 1999] and the $\delta^{13}C$ associated with the DIC in the silicate and carbonate weathering input fluxes is taken as 0.0‰ [*Kump and Arthur*, 1999]. The majority of the carbonate sedimentation flux is made up of surface dwelling foraminifera and coccolithophores. The $\delta^{13}C$ of the $CaCO_3$ sedimentation flux is thus set to be the $\delta^{13}C_{DIC}$ value of the low-latitude surface ocean box. This assumes that the bulk calcite sedimentation output flux is in isotopic equilibrium with DIC in the low-latitude surface box which typically has values in the range 1.0–2.0‰. Therefore, unless there is an additional output flux of more isotopically depleted material mean ocean $\delta^{13}C_{DIC}$ will drift toward more negative values.

[19] Records of deep Pacific Ocean benthic $\delta^{13}C_{calcite}$ over the past 5 Myr show that average values on the Myr timescale remain in the range −0.1 to +0.1‰ [*Mix et al.*, 1995a; *Wang et al.*, 2004] demonstrating that any such drift is very small in amplitude. This effective buffering of $\delta^{13}C_{DIC}$ must arise from the marine production and sedimentation of C_{org}, with an isotopic composition taken in the model as −23.0‰. The primary source of oceanic C_{org} is direct fixation of DIC though primary productivity, with a much smaller component arising through riverine input of weathered terrestrial organic material [*Hedges et al.*, 1997]. The vast majority of the C_{org} present in the surface ocean is then remineralized within the subsurface ocean leaving only a small sedimentation flux of ~0.15 GtC yr^{-1} in the modern case [*Hedges et al.*, 1997]. The dominance of the primary productivity source for marine C_{org} suggests that the best first-order parameterization of the C_{org} sedimentation flux is as a function of primary productivity. A simple linear function is used in the first instance:

$$F_{org} = k_{org}P_{surface} \quad (11)$$

The residence time of C_{org} (400 – 6000yr) [*Raymond and Bauer*, 2001] is substantially shorter than that of DIC or the period of the 400–500 kyr cycles. Thus, the organic sedimentation flux is assumed to have a negligible effect on

surface ocean DIC concentrations. The effect of temporally variability in the isotopic fraction between inorganic and organic carbon [*Rau et al.*, 1991] is also assumed to be negligible on this timescale. The value of k_{org} is selected as 0.009 such that, for all forcing parameters used, the equilibrium value of $\delta^{13}C_{DIC}$ lies in the range consistent with the observed mean over the past 5 Myr in benthic $\delta^{13}C_{calcite}$.

3. Model Runs

3.1. Scenarios PRP, TP, WEATH, and PRP/TP

[20] The global balance in marine primary production between siliceous (principally diatom) and calcareous (principally coccolithophore) phytoplankton could change according to either seasonality (as the two groups tend to live at different latitudes) [*Rickaby et al.*, 2007] or the relative supply of silica and ALK to the global ocean [*Wang et al.*, 2004]. In either case, changes will occur in the global ratio of $CaCO_3/C_{org}$ of the material entering the biological pump. Due to the different $\delta^{13}C$ values of carbon in biogenic calcite and organic matter, this could plausibly lead to fluctuations in mean ocean $\delta^{13}C_{DIC}$ [*Hoogakker et al.*, 2006; *Wang et al.*, 2004]. The "Production Ratio Parameter hypothesis" (PRP) states that variations in the global $CaCO_3/C_{org}$ value for material entering the biological pump accounts for the observed 400–500 kyr periodicities. BoxKIT treats phosphate as the sole limiting nutrient for primary productivity using a Michaelis-Menton function. Therefore, the PRP scenario is investigated through direct forcing of the $CaCO_3/C_{org}$ value associated with primary productivity in all surface boxes. The Holocene global average $CaCO_3/C_{org}$ value is taken as 0.27 and forcing amplitudes in the range 0.00–0.35 are explored.

[21] Changes in the supply to the ocean of productivity-limiting nutrients, such as phosphate, may lead to changes in total primary productivity without necessarily changing the value of $CaCO_3/C_{org.}$ The strength of the biological pump is related to the ultimate burial flux of both C_{org} and $CaCO_3$ so variations in total productivity may also affect the mean ocean $\delta^{13}C_{DIC}$ value [*Keir*, 1992; *Sigman and Boyle*, 2000]. The "Total Productivity" hypothesis (TP) states that variations in total marine primary productivity account for the observed 400–500 kyr periodicities. TP is investigated through forcing of the mean ocean phosphate concentration, |[P]|. The Holocene value for |[P]| is taken as 2.35 μmol L^{-1} and forcing amplitudes in the range 0.00–0.65 μmol L^{-1} are explored. Scenarios PRP and TP are not mutually exclusive and a series of runs involving the superposition of the two forcing mechanisms both in-phase (such that high $CaCO_3/C_{org}$ values are coincident with high total productivity) and in antiphase (such that low $CaCO_3/C_{org}$ values are coincident with high total productivity) with one another was also performed.

[22] Changes in the fluxes of weathered inorganic carbon and ALK have the potential to affect mean ocean $\delta^{13}C_{DIC}$ without directly affecting primary productivity because such changes can change the oceanic DIC/ALK ratio and the sedimentation flux of $CaCO_3$ [*Clark et al.*, 2006; *Hoogakker et al.*, 2006; *Raymo et al.*, 1997]. The "Weathering Hypothesis" (WEATH) states that variations in the flux of weathered inorganic carbon and ALK can account for the observed 400–500 kyr periodicities. WEATH is investigated by forcing variability in the silicate weathering constant k_{sil}. The modern value of k_{sil} is taken as 62,300 mol C s^{-1} [*Toggweiler*, 2008] and forcing amplitudes in the range 0–26,000 mol C s^{-1} are investigated.

[23] None of the above scenarios is dependent on the presence of glacial-interglacial cycles in climate or global ice volume. They thus all provide mechanisms consistent with the apparent persistence of the 400–500 kyr cycles across the late Mesozoic and Cenozoic greenhouse to icehouse transition. Model runs were also performed using an additional linear trend in k_{sil} to simulate the effect of a long-term Cenozoic decrease in pCO_2. A trend of 0.01 mol s^{-1} yr^{-1} in k_{sil} leads to a decrease of ~15 ppmV Myr^{-1} in pCO_2. No significant difference in the amplitude or phase of the periodic response in $\delta^{13}C_{DIC}$, pCO_2 and $[CO_3^{-2}]_{mean}$ occurs provided that mean pCO_2 does not differ from the equilibrium value by more than ± 50 ppmV in which case the model equilibrium $\delta^{13}C_{DIC}$ moves outside of the −0.1 to 0.1‰ range defined by benthic $\delta^{13}C_{calcite}$ data for the past 5 Myr. This suggests that the model output of interest here is insensitive to drift in the mean pCO_2 level on the Pleistocene timescale [*Zeebe and Caldeira*, 2008] but that this effect may become significant on the Cenozoic timescale.

3.2. Evaluating Model Sensitivity to Forcing Function Periods and Amplitudes

[24] In each simulation the model is initially spun up from the Holocene initial conditions of *Toggweiler* [2008] for 1.5 Myr, by which time equilibrium in $\delta^{13}C_{DIC}$, pCO_2 and $[CO_3^{-2}]_{mean}$ is attained. After this spin-up phase, forcing functions are activated, such that there is no discontinuity in the forced parameters. The forcing functions consist of one or more of the open system process parameters, as described above, being varied with a sinusoidal forcing function across a period of 3 Myr.

[25] Selection of both the period and amplitude to use for the forcing functions is not trivial. The dominant periodicity in the 400–500 kyr range observed in $\delta^{13}C_{calcite}$ records evolves within single downcore records across the past 5 Myr [*Wang et al.*, 2004]. Furthermore, different proxies and different core locations yield differing dominant periodicities within the 400–500 kyr range. The variation between cores is potentially related to age model uncertainties as $\delta^{13}C_{calcite}$ is not generally used as a tuning target in the creation of sediment core age models. However, the variation within single records, particularly the lengthening of dominant period toward ~500 kyr in the Pleistocene, which is seen in multiple proxies, is likely to be a real feature of the system.

[26] To explore model sensitivity to the period of the forcing, a set of initial experiments was performed using different forcing periodicities across the range 100–750 kyr. The results of these sensitivity tests are presented in full in Appendix B. A simple one to one relationship between the period of response and the forcing period used is observed but the choice of forcing period also affects the amplitude of periodic response in the parameters of interest. This effect is, however, relatively small for forcing periods in

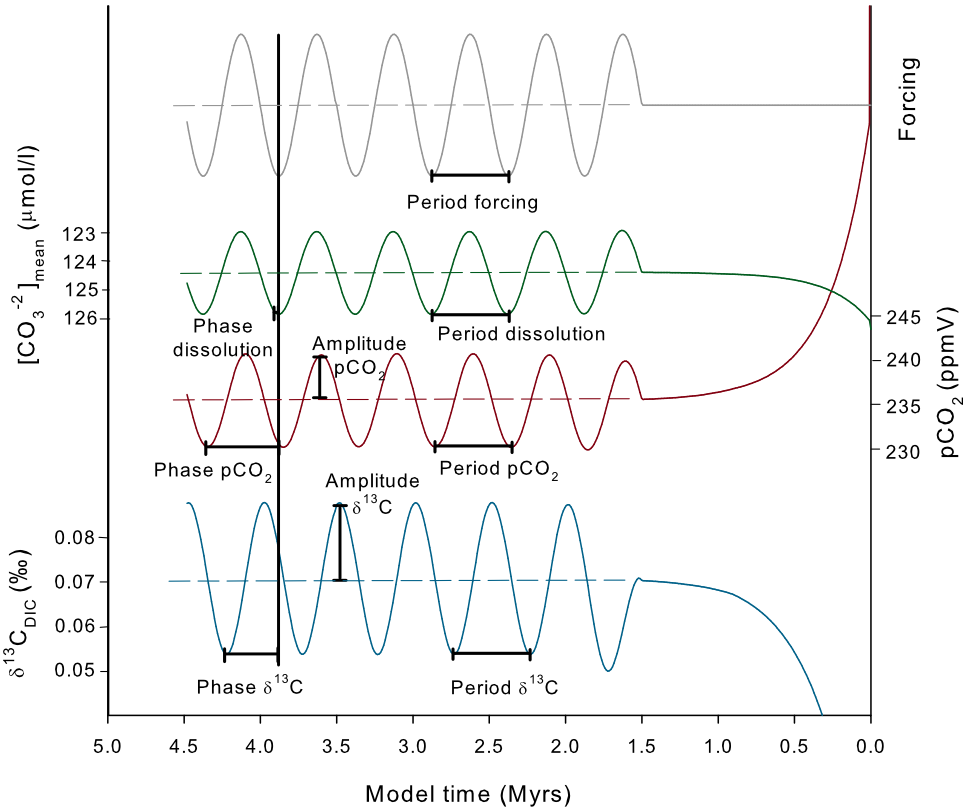

Figure 4. Sample model output for $\delta^{13}C_{DIC}$, $[CO_3^{-2}]_{mean}$ (inverted scale means that dissolution increases upward) and pCO_2 against time (in Myr after commencement of run) for an arbitrary forcing function (gray line). The definitions of the amplitude of periodic response in $\delta^{13}C_{DIC}$ and pCO_2, the periods of response in $\delta^{13}C_{DIC}$, $[CO_3^{-2}]_{mean}$ and pCO_2 and the phase of these variables in relation to the forcing are shown. The relative phase is defined such that for a positive angle the response parameter lags the forcing (as shown here). The time axis runs right to left for easier comparison of phases with those in the proxy data. Dashed lines represent the equilibrium values of the parameters.

the 400–500 kyr range. For simplicity, a single forcing period of 500 kyr is used in all subsequent model runs.

[27] Robust proxy records at an appropriate resolution over the past 5 Myr of the global ocean production ratio of $CaCO_3/C_{org}$, total primary productivity or riverine fluxes of weathered inorganic carbon and ALK do not at present exist. Therefore, experiments using a wide range of forcing function amplitudes for these variables were undertaken. Determining the mean values to use for each forcing variable presents a further difficulty. The Holocene appears to represent a maximum or near maximum in the Pleistocene ~500 kyr $\delta^{13}C_{DIC}$ cycle (Figures 1a and 2b). However, Holocene conditions do not necessarily correspond to a maximum in each of the potential forcing parameters. It is therefore necessary to experiment with a range of mean values for each forcing. In the case of a higher (lower) than Holocene long-term mean value, the amplitude of variability is defined such that the modern value represents a minima (maxima) in the forcing cycle. The results of these sensitivity tests are presented in full in Appendix B. The approach taken is to use the better constrained Holocene values as the long-term mean in each case but to limit the range of forcing amplitudes used such that the uncertainty arising from this choice of mean forcing value on the amplitude of response in $\delta^{13}C_{DIC}$ and pCO_2 is < 0.05‰ and < 5 ppmV, respectively.

4. Results

[28] In each model run, the values of $\delta^{13}C_{DIC}$, pCO_2 and $[CO_3^{-2}]_{mean}$ initially approach their respective equilibrium values during the spin-up phase (Figure 4). For the Holocene initial conditions used here, the long-term equilibrium values of $\delta^{13}C_{DIC}$ and pCO_2 are 0.06‰ and 236 ppmV, respectively. $[CO_3^{-2}]_{mean}$ is used as a qualitative proxy for ocean average carbonate preservation, such that when $[CO_3^{-2}]_{mean}$ is at a maximum, carbonate preservation (dissolution) is at a maximum (minimum). After the spin-up phase and the activation of the forcing functions, sinusoidal behavior is exhibited by $\delta^{13}C_{DIC}$, pCO_2 and $[CO_3^{-2}]_{mean}$. The model output is saved every 10 kyr throughout each 3Myr run and used to determine the periods and relative phases of the $\delta^{13}C_{DIC}$, pCO_2 and $[CO_3^{-2}]_{mean}$ response and the amplitudes of the $\delta^{13}C_{DIC}$ and pCO_2 response, as shown in Figure 4. The relative phase of the responses is

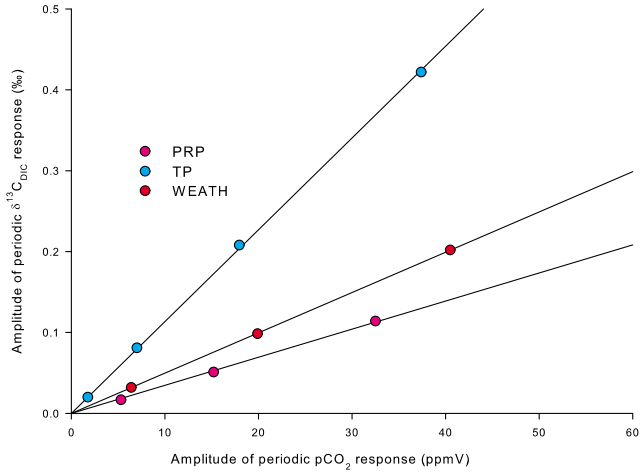

Figure 5. The relationship between the amplitude of periodic response in $\delta^{13}C_{DIC}$ and pCO_2 for different forcing amplitudes of the Production Ratio Parameter (PRP), Total Productivity, (TP), and Weathering (WEATH) hypotheses. The gradients (R_{amp}) for each regression line are shown. All forcing periods were 500 kyr, and the mean forcing amplitudes were Holocene values.

calculated instantaneously for the last full cycle present in each model run.

[29] The uncertainties in the results are directly linked to both the uncertainties in the numerical values used within the parameterization of each scenario (Appendix B) and the assumptions in the model itself. Accurate modeling of past values for $\delta^{13}C_{DIC}$, pCO_2 and $[CO_3^{-2}]_{mean}$ is not realistic given these limitations. However, first-order results regarding the sensitivity and phase of response to the various forcing mechanisms are significant against the parameterization uncertainties.

4.1. Amplitudes of Response for the PRP, TP, and WEATH Scenarios

[30] In PRP, TP and WEATH experiments using variable forcing amplitudes a linear response between the amplitudes of periodic response in $\delta^{13}C_{DIC}$ and pCO_2 is observed for each scenario (Figure 5). For PRP forcing alone, the relationship between the amplitude of response in $\delta^{13}C_{DIC}$ and pCO_2 (R_{amp}) is 0.003 ‰ ppmV^{-1}, for TP it is 0.011 ‰ ppmV^{-1} and for WEATH, 0.005‰ ppmV^{-1}.

[31] The result of a matrix of model runs (n = 50) using combinations of the forcing variables PRP and TP is presented in terms of both the amplitude of $\delta^{13}C_{DIC}$ and pCO_2 response and the ratio of these two values, R_{amp} (Figure 6). Experiments were performed with the forcing functions both in-phase (maximum $CaCO_3/C_{org}$ coincident with maximum total productivity) and in antiphase (maximum $CaCO_3/C_{org}$ coincident with minimum total productivity). The PRP/TP forcing produces a complex response in R_{amp} values across the phase space because of the different relative amplitudes and phases of the $\delta^{13}C_{DIC}$ and pCO_2 response for the two individual forcing parameters. For the pCO_2 response, the lines of equal amplitude response are parallel to |[P]|/$CaCO_3/C_{org}$ ~3.0 μmol L^{-1} and for the $\delta^{13}C_{DIC}$ response, the lines of equal amplitude response are parallel to |[P]|/$CaCO_3/C_{org}$ ~0.8 μmol L^{-1} (Figure 6). In both instances, the line of minimum response (occurring at perfect destructive interference) passes through the origin (no forcing) and the in-phase forcing space but not the antiphase one, because in the former the relative phases favor destructive interference and in the latter, constructive interference. Thus, a zone of high R_{amp} values exceeding those found in either the individual PRP or TP scenarios and centered around |[P]| ~0.4 umol L^{-1} and $CaCO_3/C_{org}$ ~ 0.1 occurs in the in-phase forcing space. However, for the antiphase PRP/TP forcing the values of R_{amp} are always between those found for the individual PRP and TP scenarios.

4.2. Periods of Response for the PRP, TP, and WEATH Scenarios

[32] The spectral properties of the $\delta^{13}C_{DIC}$ and pCO_2 output arising from model runs using forcing periods of 500 kyr were analyzed using the Analyseries software [*Paillard et al.*, 1996]. For forcing with PRP, TP, WEATH or antiphase PRP/TP the resultant output in both variables showed a single dominant periodicity at 500 ± 10 kyr (the resolution of the spectral analysis method used) in every simulation. In the case of the in-phase PRP/TP runs the dominant period of the resultant cycles in $\delta^{13}C_{DIC}$ in every simulation remained 500 ± 10 kyr. However, for the pCO_2 response a second significant spectral peak, arising through frequency doubling is seen for R_{amp} values exceeding ~0.025‰ ppmV^{-1}. In the run with a $CaCO_3/C_{org}$ forcing amplitude of 0.1 and a |[P]| forcing amplitude of 0.4 μmol L^{-1}, corresponding to near maximal R_{amp}, the 250 kyr period shows more spectral power than the 500 kyr one.

4.3. Relative Phases of Response for the PRP, TP, and WEATH Scenarios

[33] The phase relations of the model $\delta^{13}C_{DIC}$, $[CO_3^{-2}]_{mean}$ and pCO_2 responses differ significantly for the different forcing scenarios (Figure 7). For PRP, the forcing leads both pCO_2 and carbonate dissolution by 355 ± 5° and $\delta^{13}C_{DIC}$ by 260 ± 5°. In this scenario, high $CaCO_3/C_{org}$ occurs near synchronously with high pCO_2, consistent with the relative effects of carbon drawdown during photosynthesis and degassing during calcification. High $CaCO_3/C_{org}$ leads to the removal of ALK from the surface to the deep ocean leaving the parts of the ocean in which carbonate sedimentation does not occur relatively depleted in ALK. Thus, average ocean carbonate preservation is minimal at times of maximal $CaCO_3/C_{org}$. The lead of $CaCO_3/C_{org}$ over $\delta^{13}C_{DIC}$ arises as whenever $CaCO_3/C_{org}$ exceeds the equilibrium value, higher deep ocean ALK leads to more $CaCO_3$ sedimentation (in relation to that of C_{org}) and a reduction of $\delta^{13}C_{DIC}$.

[34] For TP, the forcing leads pCO_2 by 160 ± 5°, carbonate dissolution by 240 ± 5° and $\delta^{13}C_{DIC}$ by 70 ± 5°. High total primary productivity leads to drawdown of CO_2 into the biological pump (reducing atmospheric pCO_2), increased dissolution in the subsurface ocean and enhanced C_{org} sedimentation (in relation to $CaCO_3$) leading to enhanced mean ocean $\delta^{13}C_{DIC}$.

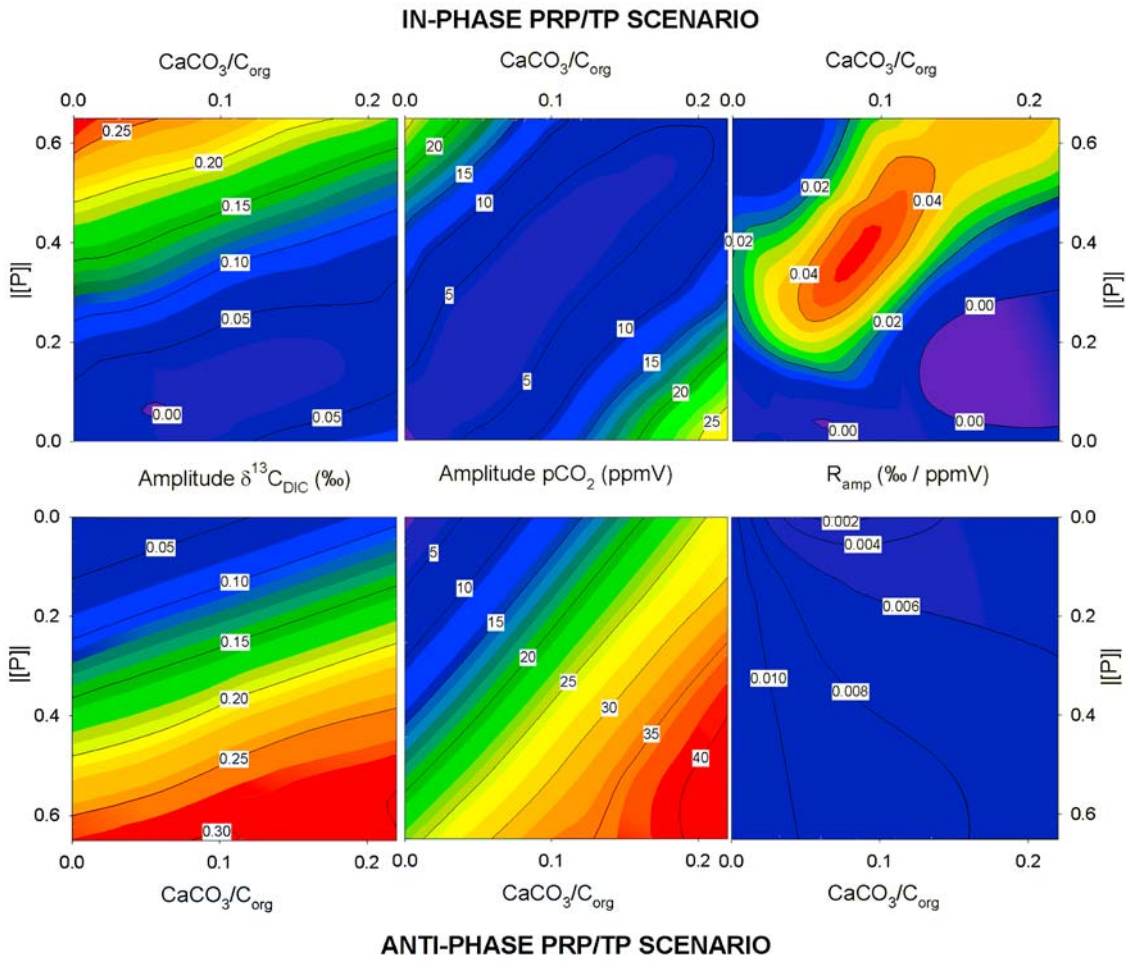

Figure 6. Contour plots of the periodic amplitude of response in (left) $\delta^{13}C_{DIC}$, (middle) pCO_2, and (right) the ratio between these values (R_{amp}) for varying amplitudes of PRP/TP forcing. Figure 6 (top) shows the response when the two forcing functions are in-phase, and Figure 6 (bottom) shows the response when they are in antiphase. Only forcing amplitudes for which the sensitivity in $\delta^{13}C_{DIC}$ response to variation in mean value used is < 0.05‰ are considered. All forcing periods were 500 kyr, and the mean forcing amplitudes were Holocene values.

[35] For WEATH, the forcing leads pCO_2 by 220 ± 5°, dissolution by 310 ± 5° and $\delta^{13}C_{DIC}$ by 240 ± 5°. The WEATH phase lags arise through the long time constant of the silicate weathering feedback. When pCO_2 exceeds the long-term equilibrium value, silicate weathering acts to lower it again adding ALK to the global ocean and thus increasing both carbonate preservation and $CaCO_3$ sedimentation (relative to that of C_{org}) which, in turn, increases $\delta^{13}C_{DIC}$. Because the carbonate sedimentation feedback is relatively fast compared to the silicate weathering one, the $\delta^{13}C_{DIC}$ response is close to being in-phase with pCO_2. The 90° phase lag of dissolution behind pCO_2 arises as whenever, pCO_2 is greater than (lower than) the long-term equilibrium value, $[CO_3^{-2}]_{mean}$ increases (decreases).

[36] In the PRP/TP scenarios, the relative phase of the $\delta^{13}C_{DIC}$, pCO_2 and carbonate dissolution responses depends on the relative amplitudes of the two forcing parameters. In the case of in-phase PRP/TP forcing it is seen that the lead of the $\delta^{13}C_{DIC}$ response over pCO_2 is in the range 90–150° for the entirety of the phase space, excepting those runs in which frequency doubling was observed in pCO_2, in which case calculation of an instantaneous lead/lag is impossible. The magnitude of the phase lag approaches ~90° as either forcing amplitude approaches zero and increases with the amplitudes of both forcing functions. The carbonate dissolution response remains close to in-phase with the pCO_2 response, as in the PRP scenario. In the case of antiphase forcing with PRP/TP, the phase lag between $\delta^{13}C_{DIC}$ and pCO_2 is always 90±10° regardless of the forcing amplitudes used and carbonate dissolution again remains close to in-phase with the pCO_2 response.

5. Discussion

5.1. Proxy Constraint on the Amplitude of Response in $\delta^{13}C_{DIC}$ and pCO_2

[37] The three proxy records used for comparison with the model output are the ODP Site 1143 benthic $\delta^{13}C_{calcite}$

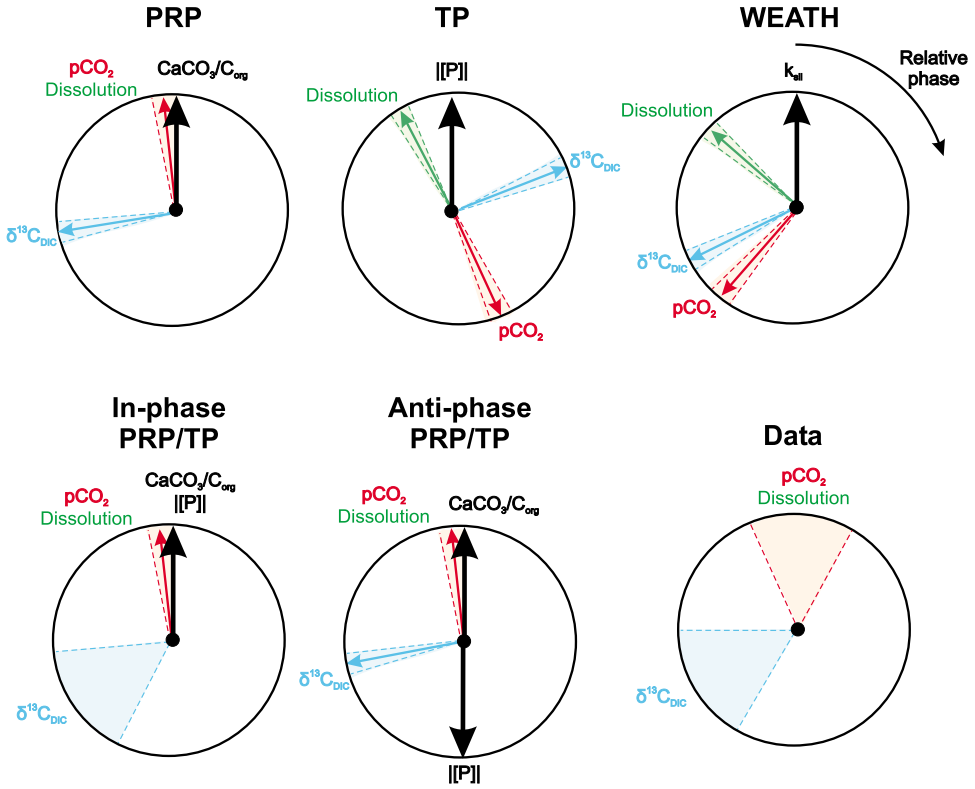

Figure 7. Schematic phase wheel plots for the $\delta^{13}C_{DIC}$, carbonate dissolution and pCO_2 responses to the PRP, TP, WEATH, in-phase PRP/TP, and antiphase PRP/TP forcing scenarios. Positive relative phase is defined in a clockwise sense, such that the $\delta^{13}C_{DIC}$ response lags the forcing but leads the pCO_2 response in the TP scenario. The relative phase of the forced parameter(s) (thick black arrows) is set to zero, except in the antiphase PRP/TP scenario in which $CaCO_3/C_{org}$ forcing is set to zero and |[P]| forcing to 180°. The uncertainties in the model phases arise from the resolution imposed by the time step used (±5 kyr). In plots where the dissolution response is not visible, it is synchronous with the pCO_2 response. The bottom right plot shows the known data constraints, with the pCO_2/carbonate dissolution phase set arbitrarily to zero.

record [*Wang et al.*, 2004] over the past 5 Myr, the Antarctic composite ice core pCO_2 record [*European Project for Ice Coring in Antarctica* (*EPICA*) *Community Members*, 2004; *Lüthi et al.*, 2008; *Petit et al.*, 1999; *Siegenthaler et al.*, 2005] over the past 0.8 Myr and finally, carbonate preservation inferred from a composite Indian Ocean GSI record over the past 1.5 Myr [*Bassinot et al.*, 1994] (Figure 2). Benthic $\delta^{13}C_{calcite}$ in certain species of foraminifera acts as a proxy for deep water $\delta^{13}C_{DIC}$ [*Duplessy et al.*, 1984; *McCorkle and Keigwin*, 1994] and the ODP 1143 record clearly demonstrates the 400–500 kyr periodicities over the past 5 Myr hence its selection as the $\delta^{13}C_{DIC}$ proxy comparison.

[38] The ODP 1143 $\delta^{13}C_{calcite}$ record shows considerable temporal variability in amplitude between individual 400–500 kyr cycles. However, Gaussian filtering using a 350 kyr bandwidth filter demonstrates that the amplitude of variability in the > 350 kyr range always lies within the range 0.05–0.15‰ over the past 5 Myr (Figure 1a). The same filter applied to the Antarctic pCO_2 record demonstrates that the amplitude of variability in the > 350 kyr range over the past 0.8 Myr is < 10 ppmV (Figure 2b). The relatively short duration of the pCO_2 record limits the potential for comparison of the two records. However, the apparent absence of significant 400–500 kyr periodicity from proxy records of Plio-Pleistocene equatorial Pacific sea surface temperature [*Dekens et al.*, 2008; *Lawrence et al.*, 2006] suggests there is no clear reason to suppose the amplitude of pCO_2 variability at these periods to be greater prior to 0.8 Ma. Interestingly, certain extratropical sea surface temperature records do show evidence for variability on these timescales but this is believed to be related to subtropical front movement and decoupled from pCO_2 variability [*Bard and Rickaby*, 2009]. If the 10 ppmV value from the Antarctica record is taken as a best guess upper bound to the Plio-Pleistocene pCO_2 cycle amplitude and using the range of $\delta^{13}C_{DIC}$ cycle amplitudes from the ODP 1143 $\delta^{13}C_{calcite}$ record, the range of minimum acceptable values for model R_{amp} is 0.005–0.015‰ $ppmV^{-1}$.

[39] All of the scenarios experimented with here are capable of generating periodic response of 0.05−0.15‰ amplitude in $\delta^{13}C_{DIC}$. However, it is a pronounced feature of the model output that most scenarios also predict relatively large amplitude cycles at the same period in

pCO_2 - they have relatively low R_{amp} values (Figure 5). Both the PRP (R_{amp} = 0.003‰ $ppmV^{-1}$) and WEATH (R_{amp} = 0.005‰ $ppmV^{-1}$) scenarios produce unacceptably large amplitude pCO_2 variability across the entire observed range of $\delta^{13}C_{DIC}$ cycle amplitudes. The TP scenario (R_{amp} = 0.011‰ $ppmV^{-1}$) provides the closest match to the observed relative amplitudes but even this cannot reproduce the upper end $\delta^{13}C_{DIC}$ cycle amplitudes without also generating pCO_2 response > 10 ppmV.

[40] Much of both the in-phase and antiphase PRP/TP phase spaces have R_{amp} values > 0.005‰ $ppmV^{-1}$ (Figure 6). However, in the antiphase case values are always lower than for TP alone (R_{amp} = 0.011‰ $ppmV^{-1}$) and only a small subset of the region with R_{amp} > 0.005‰ $ppmV^{-1}$ is consistent with a pCO_2 response of < 10 ppmV. For the in-phase case these two regions are broadly coincident and of all the scenarios evaluated here, only in-phase PRP/TP is able to produce the entire observed range of $\delta^{13}C_{DIC}$ amplitudes without also generating pCO_2 response > 10 ppmV.

5.2. Proxy Constraint on the Phase of the Response

[41] Comparison in the time domain of the > 350 kyr period component of the ODP 1143 $\delta^{13}C_{calcite}$, Antarctic composite pCO_2 and Indian Ocean GSI records over the past 1.5 Myr demonstrates irregular "pseudocycles" with a period of 500 ± 100 kyr in all records (Figure 2b). The pCO_2 record and dissolution index are close to being in phase over the past 0.8 Myr, suggesting that the longer GSI record may be used as a first-order guide to the relative phase of $\delta^{13}C_{DIC}$ and pCO_2 over the past 1.5 Myr. Over this period, the $\delta^{13}C_{DIC}$ cycles lead carbonate dissolution (and by inference pCO_2) by 90–150° (Figure 7). The uncertainties involved in correlating the various age models for the proxy data sets is of the order of 5–10 kyr and would not change the first-order relationships between the variables.

[42] Of the single forcing function scenarios, PRP provides a lead of $\delta^{13}C_{DIC}$ over pCO_2 and carbonate dissolution of ~90°, consistent with the proxy data (Figure 7). TP provides the same lead of $\delta^{13}C_{DIC}$ over pCO_2 but carbonate dissolution is in near antiphase with pCO_2. WEATH provides $\delta^{13}C_{DIC}$ response close to in-phase with pCO_2 and both leading dissolution by ~90°. In the PRP/TP scenario (both in-phase and in antiphase) the relative phase criteria are always met. Therefore, the forcing scenarios most consistent with the phase constraints are the PRP and PRP/TP scenarios.

[43] The phases of the $\delta^{13}C_{DIC}$, pCO_2 and carbonate preservation responses in relation to the forcing functions used are also very different for the three scenarios. This is not however used as a discriminating test due to the difficulty of directly relating the phase of the forcing parameters used in the model to a proxy or orbital variable.

5.3. Proxy Constraint on the Period of the Response

[44] The model does not generate significant phase modulation and to generate a 500 kyr periodicity requires a 500 kyr forcing function. The frequency-doubling behavior seen for pCO_2 at high R_{amp} values in the PRP/TP scenario is the only exception to this. As such behavior is associated exclusively with very low amplitudes of model pCO_2 response it is unlikely that even the availability of longer proxy records will allow its evaluation. As such, this aspect of model output is not considered useful for the discrimination of different hypotheses.

[45] A significant discrepancy therefore exists between the observed Pleistocene ~500 kyr periodicity and the proposed origin of the forcing in the orbital eccentricity cycle at 413 kyr. The middle-late Pleistocene is uniquely characterized by the ~100 kyr mode of glacial-interglacial climate variability and it is possible that this relatively high amplitude periodicity interferes with the last two $\delta^{13}C_{DIC}$ and carbonate preservation cycles such that the apparent periodicity is greater than a "true" underlying period at 413 kyr. Within such an interpretation, the proposed global negative $\delta^{13}C_{DIC}$ shift during the Middle Pleistocene Transition [*Raymo et al.*, 1997] may act to enhance the "natural" $\delta^{13}C_{DIC}$ cycle minima (Figure 2).

5.4. Evaluating the Different Scenarios

[46] Of the proxy data constraints presented here only the amplitude of the $\delta^{13}C_{DIC}$ cycles, as inferred from $\delta^{13}C_{benthic}$, is comparable to model output across more than 1.5 Myr. Taking this constraint alone, any of the investigated forcing mechanisms is capable of generating the appropriate amplitude of $\delta^{13}C_{DIC}$ response. However, if it is assumed that the amplitude of observed > 350 kyr band variability seen in pCO_2 and the in-phase relationship seen between carbonate dissolution and pCO_2 over the past 0.8 Myr are representative of longer-term variability, then the scenarios may be discriminated between at quite a fine level.

[47] The two most useful constraints used for evaluating the different scenarios are "the relative amplitude constraint": $\delta^{13}C_{DIC}$ cycles of amplitude 0.05–0.15 ‰ should be generated without the amplitude of pCO_2 variability exceeding 10 ppmV and "the relative phase constraint": the $\delta^{13}C_{DIC}$ cycles should lead the pCO_2 cycles by 90–150° and the carbonate dissolution cycles should be close to in-phase with pCO_2.

[48] The WEATH scenario fails both the phase and amplitude constraints and is therefore rejected. Furthermore, the sensitivity of the model output to changes in the system parameters is substantially greater when forced with WEATH than with the biological parameters. Thus, more detailed investigation of the role played by the weathering of inorganic material requires better data constraints before it can be further evaluated.

[49] The TP scenario fulfils the amplitude constraint but fails the phase constraint. In contrast, the PRP and antiphase PRP/TP scenarios fulfill the phase constraint but fail the amplitude constraint. It is likely, however, that the amplitude constraint is more sensitive than the phase constraint to both the model parameters and the limited availability of pCO_2 data. Thus, if a single forcing parameter is sought as the origin of the 400–500 kyr periodicities, the PRP scenario is favored.

[50] Of all the scenarios investigated here, only the in-phase PRP/TP scenario fulfils both constraints simultaneously. The subset of the in-phase PRP/TP phase space consistent with both the amplitude and phase constraints is broadly defined by the forcing amplitudes

of $CaCO_3/C_{org} > 0.02$ and $|[P]| > 0.1$ μmol L^{-1}. Thus, the minimum forcing values needed to satisfy the constraints are relatively small, representing variability of 7 and 4%, respectively, from the Holocene mean values. Significantly, the model is relatively insensitive to parameter choice and initial conditions when forced with the biological component of the carbon cycle (Appendix B). As the proxy data constraints are met using a fairly wide range of forcing functions in the PRP/TP space, the model suggests that changes in inorganic weathering of DIC and ALK are not necessary to explain the observed periodicities in the carbon cycle.

[51] The model results suggest that the relatively low amplitude of pCO_2 variability and hence climatic response in the 400–500 kyr band may arise from the counterbalance on the global scale of high relative carbonate (principally coccolithophore as opposed to diatom) production with high total marine productivity. This is consistent with both previous modeling studies [*Barker et al.*, 2006] and observations that carbonate dissolution, which is close to in-phase with the forcing functions for the in-phase PRP/TP scenario (Figure 7) is broadly in-phase with Pleistocene coccolithophore bloom productivity [*Rickaby et al.*, 2007]. The origins of secular variability in coccolithophore productivity across the Pleistocene have been proposed to relate to variations in silica leakage from the high-latitude Southern Ocean [*Barker et al.*, 2006; *Matsumoto et al.*, 2002; *Rickaby et al.*, 2007]. In such a scenario, the global ocean oscillates between states of intense low-latitude coccolithophore and polar diatom productivity (high total primary productivity) and periods of diatoms blooming at low latitudes but limited high-latitude diatom productivity (low total primary productivity) [*Rickaby et al.*, 2007].

[52] The ultimate origin of this variability has been proposed to be the orbital eccentricity cycle and its effect on seasonality and thus silica utilization in the Southern Ocean [*Brzezinski et al.*, 2002; *Matsumoto et al.*, 2002; *Matsumoto and Sarmiento*, 2008]. Across the middle-late Pleistocene the available proxy data seems to support this, with the eccentricity minima at ~0.4 Ma coinciding with the carbonate dissolution and coccolithophore bloom production maxima [*Rickaby et al.*, 2007] (Figure 2b). However, when evaluated over the past 1.5 Myr, the difference in dominant period between the eccentricity and various proxy records means that no clear phase relationship is discernible (Figure 2b). Furthermore, comparison between the ODP 1143 $\delta^{13}C_{calcite}$ and eccentricity records over the past 5 Myr again yields no clear phase relationship (Figure 1a).

[53] One possible explanation for this is that the eccentricity cycle interacts with the carbon cycle on this timescale not through seasonality but through changes in the weathered fluxes of silica and ALK to the global ocean [*Wang et al.*, 2004]. This latter mechanism may well involve a significant and temporally variable phase lag between changes in eccentricity and the subsequent availability of the nutrients in the global ocean. The present model results support the viability of a mechanism such as silica leakage in generating the observed $\delta^{13}C_{DIC}$ cycles but the absence of phase modulation behavior suggests that, if orbital eccentricity is the ultimate origin of the cycles, then the relationship between eccentricity and the availability of nutrients in the ocean must be nondirect and temporally variable.

5.5. Limitations of the Model

[54] The present study constitutes very much a first attempt toward sensitivity analysis of the long-term ocean carbon cycle to open system forcing. It clearly demonstrates the viability of fluctuations in $CaCO_3/C_{org}$ and total primary productivity as causes of the observed $\delta^{13}C_{DIC}$ cycles. However, significant limitations in the availability of data to both parameterize and test the model prevent more accurate treatment of the problem. The future development of globally averaged (stacked) Plio-Pleistocene proxy records, such as has now been done for $\delta^{13}C_{calcite}$ for the late Pleistocene [*Oliver et al.*, 2009] would greatly aid future model-data comparisons of this type.

[55] The most significant source of likely error in the model itself is likely to be in the parameterization of the C_{org} cycle. In order for $\delta^{13}C_{DIC}$ to remain buffered within the observed limits, it is necessary that the C_{org} cycle remains closely coupled to the inorganic one on the timescales of interest. More sophisticated treatment involving both inputs of weathered terrestrial C_{org} and the role played by C_{org} in sediment surface chemistry may well reveal behavior beyond the scope of the present model and allow direct comparison of model output with carbonate preservation records. Also, an entirely alternative origin for the $\delta^{13}C_{DIC}$ cycles may be long-term fluctuations in the size of the terrestrial biosphere, an option not investigated here. A more realistic implementation of primary productivity would account for spatial variability in the $CaCO_3/C_{org}$ production and rain rate ratios. The incorporation of shallow water carbonate sedimentation and dissolution would be a useful refinement to the model and allow the evaluation of the role played by the expansion of coral reefs in the Pleistocene.

[56] A more general additional source of uncertainty arises from the fact that riverine fluxes are not in a true steady state on the glacial-interglacial timescale [*Vance et al.*, 2009]. It is plausible that the change from ~413 to ~500 kyr $\delta^{13}C_{DIC}$ cycles observed over the Plio-Pleistocene may arise from the interaction between a single, eccentricity driven periodicity and the superimposed glacial-interglacial variability. The absence of glacial-interglacial dynamics and the change in their mode across the Middle Pleistocene Transition may thus explain the inability of the present model to generate phase modulation.

6. Conclusions

[57] A 7 box ocean-atmosphere model was adapted to include the processes necessary to study the ocean carbon system on > 100 kyr timescales and then used to undertake sensitivity analysis of various hypothetical origins of the observed 400–500 kyr periodicities present in the Cenozoic ocean carbon cycle. The model is able to produce appropriate amplitude cycles in $\delta^{13}C_{DIC}$ when forced by periodic changes in the oceanic production ratio of $CaCO_3/C_{org}$, the weathering flux of continental inorganic carbon or total ocean primary productivity.

[58] In model runs using only one of the above forcing mechanisms, only forcing with the global production ratio of $CaCO_3/C_{org}$ is able to reproduce the observed phase relationship between $\delta^{13}C_{DIC,}$ carbonate preservation and pCO_2 over the past 1.5 Myr. However, the use of such forcing to reproduce the observed amplitude of $\delta^{13}C_{DIC}$ variability leads to larger amplitudes pCO_2 cycles than is consistent with available data. Forcing of the model with both the global production ratio of $CaCO_3/C_{org}$ and total primary productivity is able to replicate both the relative amplitudes and phases of response. This suggests that the relatively low amplitude of pCO_2 and hence climatic response in the 400–500 kyr band arises from the counterbalance on the global scale of high relative carbonate (principally coccolithophore as opposed to diatom) production with high total marine productivity.

[59] The simple model investigated here demonstrates that relatively small variations in the relative and total availability of different nutrients in the global ocean could account for the 400–500 kyr $\delta^{13}C_{DIC}$ periodicity. It cannot, however, explain any degree of phase modulation between the forcing and response. If the ultimate origin of the $\delta^{13}C_{DIC}$ cycles is orbital eccentricity then a significant discrepancy remains between the eccentricity period of 413 kyr and the observed ~500 kyr $\delta^{13}C_{DIC}$ periodicity seen in the Pleistocene.

Appendix A: Model Calculation of $\delta^{13}C_{DIC}$ and pCO_2

[60] The $\delta^{13}C_{DIC}$ terms are calculated using $X_i = \delta^{13}C_{DIC_i} \times [DIC]_i$ and $F = \delta^{13}C_{DIC\ (flux)} \times F_{(carbon)}$ in equation (1). In the latter expression, $\delta^{13}C_{DIC\ (flux)}$ is the isotopic composition of the open system flux (e.g., sedimentation) and $F_{(carbon)}$ is the flux of carbon (either DIC or C_{org}) in mol s^{-1}. The atmospheric pCO_2 value is computed as a secondary variable by subtracting the amount of DIC in each ocean box from the total amount in the entire system at that time. The total amount of DIC in the system at time T ($DIC_{t=T}$) is evaluated based on the initial condition starting mean ocean [DIC] value ($[DIC]_{t=0}$) and the open system fluxes using $DIC_{t=T} = [DIC]_{t=0}\ V_{total} + \int_{t=o}^{t=T} (F^{IN} - F^{OUT})dt$. The atmospheric $\delta^{13}C$ value is computed in an analogous way using $X_{t=0} = \delta^{13}C_{DIC_{t=0}} \times [DIC]_{t=0}$ in place of $DIC_{t=0}$ ($\delta^{13}C_{DIC\ t=0}$ is set to be 0.0‰) and $F^{IN/OUT} = \delta^{13}C_{DIC\ (flux)} \times F_{(carbon)}$ in place of $F^{IN/OUT}$.

Appendix B: Model Sensitivity to Variations in the Mean Forcing Function Values and Periods

[61] Initial model experiments in which the forcing period for PRP, TP and WEATH forcing was varied across the range 100–750 kyr show a linear scaling of the period of response in $\delta^{13}C_{DIC}$, $[CO_3^{-2}]_{mean}$ and pCO_2. However, the amplitude of $\delta^{13}C_{DIC}$ and pCO_2 response is also dependent on the period of forcing used. This dependence produces an uncertainty in the amplitude of $\delta^{13}C_{DIC}$ response of 0.03‰ in the case of the TP scenario and < 0.005‰ for both the PRP and WEATH scenarios for forcing periods in the range 400–500 kyr. The uncertainty in pCO_2 response for the same period range is 5 ppmV for WEATH and < 1 ppmV for PRP and TP. These uncertainties, excepting the effect on pCO_2 with WEATH, are relatively small compared to the variations caused by the different forcing amplitudes experimented with.

[62] In all three of the PRP, TP and WEATH scenarios, the use of the Holocene value as the mean for the forced parameter leads to a strong linear correlation between the amplitude of forcing and the amplitude of responses in $\delta^{13}C_{DIC}$ and pCO_2. In contrast, use of mean values either above or below the modern value show a nonlinear response principally due to the retention of the modern boundary condition-tuned value of k_{org}. Mean forcing values in the range 0.14 – 0.41 for $CaCO_3/C_{org}$, 1.35 – 3.35 μmol L^{-1} for |[P]| and 40,000 – 100,000 mol C s^{-1} for k_{sil} were investigated. For amplitudes up to 0.35 for $CaCO_3/C_{org}$, 0.65 μmol L^{-1} for |[P]| and 26,000 mol C s^{-1} for k_{sil} the uncertainty in $\delta^{13}C_{DIC}$ response arising from the choice of mean forcing value used is < 0.05‰. For the same forcing amplitudes the uncertainty in pCO_2 response arising from the choice of mean forcing value used is 2, 5, and 5 ppmV, respectively.

[63] **Acknowledgments.** Elisabeth Michel and Ros Rickaby are thanked for useful discussions of the work. Thoughtful reviews from two anonymous reviewers greatly improved the manuscript. This work was undertaken with funding from an Entente Cordiale scholarship to T. Russon. This is LSCE contribution 4102.

References

Archer, D., and E. Maier-Reimer (1994), Effect of deep-sea sedimentary calcite preservation on atmospheric CO_2 concentration, *Nature*, *367*, 260–263, doi:10.1038/367260a0.

Archer, D., A. Winguth, D. Lea, and N. Mahowald (2000), What caused the glacial/interglacial atmospheric pCO_2 cycles?, *Rev. Geophys.*, *38*(2), 159–189, doi:10.1029/1999RG000066.

Bard, E., and R. E. M. Rickaby (2009), Migration of the subtropical front as a modulator of glacial climate, *Nature*, *460*(7253), 380–383, doi:10.1038/nature08189.

Barker, S., D. Archer, L. Booth, H. Elderfield, J. Henderiks, and R. E. M. Rickaby (2006), Globally increased pelagic carbonate production during mid-Brunhes dissolution interval and the CO_2 paradox of the MIS 1, *Quat. Sci. Rev.*, *25*(23–24), 3278–3293, doi:10.1016/j.quascirev.2006.07.018.

Bassinot, F. C., L. Beaufort, E. Vincent, L. D. Labeyrie, F. Rostek, P. J. Muller, X. Quidelleur, and Y. Lancelot (1994), Coarse fraction fluctuations in Pelagic carbonate sediments from the tropical Indian Ocean: A 1500 kyr record of carbonate dissolution, *Paleoceanography*, *9*(4), 579–600, doi:10.1029/94PA00860.

Berger, A., and M. F. Loutre (1991), Insolation values for the climate of the last 10,000,000 years, *Quat. Sci. Rev.*, *10*(4), 297–317, doi:10.1016/0277-3791(91)90033-Q.

Berner, E. K., and R. A. Berner (1987), *The Global Water Cycle: Geochemistry and Environment*, Prentice Hall, N. J.

Berner, R. A., A. C. Lasaga, and R. M. Garrels (1983), The carbonate-silicate geochemical cycle and its effect on atmospheric carbon-dioxide over the past 100 million years, *Am. J. Sci.*, *283*(7), 641–683.

Bickert, T., W. H. Berger, S. Burke, H. Schmidt, and G. Wefer (1993), Late Quaternary stable isotope record of Benthic foraminifers: Sites 805 and 806, Ontong Java Plateau, *Proc. Ocean Drill. Program, Sci. Results*, *130*, 411–420.

Brzezinski, M. A., C. J. Pride, V. M. Franck, D. M. Sigman, J. L. Sarmiento, K. Matsumoto, N. Gruber, G. H. Rau, and K. H. Coale (2002), A switch from $Si(OH)_4$ to $NO3^-$ depletion in the glacial Southern Ocean, *Geophys. Res. Lett.*, *29*(12), 1564, doi:10.1029/2001GL014349.

Clark, P. U., D. Archer, D. Pollard, J. D. Blum, J. A. Rial, V. Brovkin, A. C. Mix, N. G. Pisias, and M. Roy (2006), The middle Pleistocene transition: Characteristics. mechanisms, and implications for long-term changes in atmospheric pCO_2, *Quat. Sci. Rev.*, *25*(23–24), 3150–3184, doi:10.1016/j.quascirev.2006.07.008.

Crowley, T. J. (1995), Ice age terrestrial carbon changes revisited, *Global Biogeochem. Cycles*, *9*(3), 377–389, doi:10.1029/95GB01107.

Dekens, P. S., A. C. Ravelo, M. D. McCarthy, and C. A. Edwards (2008), A 5 million year comparison of Mg/Ca and alkenone paleothermometers, *Geochem. Geophys. Geosyst.*, *9*, Q10001, doi:10.1029/2007GC001931.

Duplessy, J. C., N. J. Shackleton, R. K. Matthews, W. Prell, W. F. Ruddiman, M. Caralp, and C. H. Hendy (1984), ^{13}C record of Benthic foraminifera in the last interglacial ocean: Implications for the carbon cycle and the global deep water circulation, *Quat. Res.*, *21*(2), 225–243, doi:10.1016/0033-5894(84)90099-1.

European Project for Ice Coring in Antarctica (EPICA) Community Members (2004), Eight glacial cycles from an Antarctic ice core, *Nature*, *429*(6992), 623–628, doi:10.1038/nature02599.

Head, M. J., and P. L. Gibbard (2005), Early middle Pleistocene transitions: An overview and recommendation for the defining boundary, *Geol. Soc. Spec. Publ.*, *247*, 1–18.

Hedges, J. I., R. G. Keil, and R. Benner (1997), What happens to terrestrial organic matter in the ocean?, *Org. Geochem.*, *27*(5–6), 195–212, doi:10.1016/S0146-6380(97)00066-1.

Herbert, T. D. (1997), A long marine history of carbon cycle modulation by orbital-climatic changes, *Proc. Natl. Acad. Sci. U. S. A.*, *94*(16), 8362–8369, doi:10.1073/pnas.94.16.8362.

Herbert, T. D., R. F. Stallard, and A. G. Fischer (1986), Anoxic events, productivity rhythms, and the orbital signature in a mid-Cretaceous deep-sea sequence from central Italy, *Paleoceanography*, *1*(4), 495–506, doi:10.1029/PA001i004p00495.

Hoogakker, B. A. A., E. J. Rohling, M. R. Palmer, T. Tyrrell, and R. G. Rothwell (2006), Underlying causes for long-term global ocean $\delta^{13}C$ fluctuations over the last 1.20 Myr, *Earth Planet. Sci. Lett.*, *248*(1–2), 15–29, doi:10.1016/j.epsl.2006.05.007.

Imbrie, J., et al. (1992), On the structure and origin of major glaciation cycles: 1. Linear responses to Milankovitch forcing, *Paleoceanography*, *7*(6), 701–738, doi:10.1029/92PA02253.

Imbrie, J., et al. (1993), On the structure and origin of major glaciation cycles: 2. The 100,000-year cycle, *Paleoceanography*, 8(6), 699–735, doi:10.1029/93PA02751.

Keigwin, L. D., and E. A. Boyle (1985), Carbon isotopes in deep-sea benthic foraminifera: Precession and changes in low-latitude biomass, in *The Carbon Cycle and Atmospheric CO_2: Natural Variations Archean to Present*, edited by E. T. Sundquist and W. Broecker, pp. 319–328, AGU, Washington, D. C.

Keir, R. (1992), Climate change: Packing away carbon isotopes, *Nature*, *357*(6378), 445–446, doi:10.1038/357445a0.

Kohler, P., and R. Bintanja (2008), The carbon cycle during the mid-Pleistocene transition: The Southern Ocean decoupling hypothesis, *Clim. Past*, *4*, 311–322.

Kump, L. R., and M. A. Arthur (1999), Interpreting carbon-isotope excursions: Carbonates and organic matter, *Chem. Geol.*, *161*(1–3), 181–198, doi:10.1016/S0009-2541(99)00086-8.

Lawrence, K. T., Z. H. Liu, and T. D. Herbert (2006), Evolution of the eastern tropical Pacific through Plio-Pleistocene glaciation, *Science*, *312*(5770), 79–83, doi:10.1126/science.1120395.

Li, G. J., J. F. Ji, J. Chen, and D. B. Kemp (2009), Evolution of the Cenozoic carbon cycle: The roles of tectonics and CO_2 fertilization, *Global Biogeochem. Cycles*, *23*, GB1009, doi:10.1029/2008GB003220.

Lüthi, D., et al. (2008), High-resolution carbon dioxide concentration record 650,000–800,000 years before present, *Nature*, *453*(7193), 379–382, doi:10.1038/nature06949.

Marchitto, T. M., J. Lynch-Stieglitz, and S. R. Hemming (2005), Deep pacific $CaCO_3$ compensation and glacial-interglacial atmospheric CO_2, *Earth Planet. Sci. Lett.*, *231*(3–4), 317–336, doi:10.1016/j.epsl.2004.12.024.

Marty, B., and I. N. Tolstikhin (1998), CO_2 fluxes from mid-ocean ridges, arcs and plumes, *Chem. Geol.*, *145*(3–4), 233–248, doi:10.1016/S0009-2541(97)00145-9.

Matsumoto, K., and J. L. Sarmiento (2008), A corollary to the silicic acid leakage hypothesis, *Paleoceanography*, *23*, PA2203, doi:10.1029/2007PA001515.

Matsumoto, K., J. L. Sarmiento, and M. A. Brzezinski (2002), Silicic acid leakage from the Southern Ocean: A possible explanation for glacial atmospheric pCO_2, *Global Biogeochem. Cycles*, *16*(3), 1031, doi:10.1029/2001GB001442.

McCorkle, D. C., and L. D. Keigwin (1994), Depth profiles of $\delta^{13}C$ in bottom water and core top C. *Wuellerstorfi* on the Ontong Java Plateau and Emperor Seamounts, *Paleoceanography*, *9*(2), 197–208, doi:10.1029/93PA03271.

Michel, E., L. D. Labeyrie, J. C. Duplessy, N. Gorfti, M. Labracherie, and J. L. Turon (1995), Could deep sub-Antarctic convection feed the world deep basins during the Last Glacial Maximum, *Paleoceanography*, *10*(5), 927–941, doi:10.1029/95PA00978.

Mix, A. C., J. Le, and N. J. Shackleton (1995a), Benthic foraminiferal stable isotope stratigraphy of Site 846: 0–1.8 Ma, *Proc. Ocean Drill. Program Sci. Results*, *138*, 839–856.

Mix, A. C., N. G. Pisias, W. Rugh, J. Wilson, A. Morey, and T. Hagelberg (1995b), Benthic foraminiferal stable isotope record from site 849, 0–5 Ma: Local and global climate changes, *Proc. Ocean Drill. Program Sci. Results*, *138*, 371–412.

Moore, T. C., N. G. Pisias, and D. A. Dunn (1982), Carbonate time series of the Quaternary and Late Miocene sediments in the Pacific Ocean: a spectral comparison, *Mar. Geol.*, *46*(3–4), 217–233, doi:10.1016/0025-3227(82)90081-0.

Oliver, K. I. C., B. A. A. Hoogakker, S. Crowhurst, G. M. Henderson, R. E. M. Rickaby, N. R. Edwards, and H. Elderfield (2009), A synthesis of marine sediment core $\delta^{13}C$ data over the last 150 000 years, *Clim. Past Discuss.*, *5*, 2497–2554.

Paillard, D. (1995), *Modèles simplifiés pour l'étude de la variabilité de la circulation thermohaline au cours des cycles glaciaire-interglaciaire*, Ph.D. diss., Univ. Paris XI, Orsay, France.

Paillard, D., L. Labeyrie, and P. Yiou (1996), Macintosh program performs time-series analysis, *Eos Trans. AGU*, *77*, 379, doi:10.1029/96EO00259.

Palike, H., R. D. Norris, J. O. Herrle, P. A. Wilson, H. K. Coxall, C. H. Lear, N. J. Shackleton, A. K. Tripati, and B. S. Wade (2006), The heartbeat of the Oligocene climate system, *Science*, *314*(5807), 1894–1898, doi:10.1126/science.1133822.

Petit, J. R., et al. (1999), Climate and atmospheric history of the past 420,000 years from the Vostok ice core, Antarctica, *Nature*, *399*(6735), 429–436, doi:10.1038/20859.

Rau, G. H., P. N. Froelich, T. Takahashi, and D. J. D. Marais (1991), Does sedimentary organic $\delta^{13}C$ record variations in Quaternary ocean $[CO_2(aq)]$?, *Paleoceanography*, *6*(3), 335–347, doi:10.1029/91PA00321.

Raymo, M. E., and W. F. Ruddiman (1992), Tectonic forcing of Late Cenozoic climate, *Nature*, *359*(6391), 117–122, doi:10.1038/359117a0.

Raymo, M. E., D. W. Oppo, and W. Curry (1997), The mid-Pleistocene climate transition: A deep sea carbon isotopic perspective, *Paleoceanography*, *12*(4), 546–559, doi:10.1029/97PA01019.

Raymo, M. E., L. E. Lisiecki, and K. H. Nisancioglu (2006), Plio-Pleistocene ice volume, Antarctic climate, and the global $\delta^{18}O$ record, *Science*, *313*(5786), 492–495, doi:10.1126/science.1123296.

Raymond, P. A., and J. E. Bauer (2001), Riverine export of aged terrestrial organic matter to the North Atlantic Ocean, *Nature*, *409*(6819), 497–500, doi:10.1038/35054034.

Rea, D. K., and M. Leinen (1985), Neogene history of the calcite compensation depth and Lysocline in the South Pacific Ocean, *Nature*, *316*(6031), 805–807, doi:10.1038/316805a0.

Rial, J. A. (2004), Earth's orbital eccentricity and the rhythm of the Pleistocene ice ages: The concealed pacemaker, *Global Planet. Change*, *41*(2), 81–93, doi:10.1016/j.gloplacha.2003.10.003.

Rickaby, R. E. M., E. Bard, C. Sonzogni, F. Rostek, L. Beaufort, S. Barker, G. Rees, and D. P. Schrag (2007), Coccolith chemistry reveals secular variations in the global ocean carbon cycle?, *Earth Planet. Sci. Lett.*, *253*(1–2), 83–95, doi:10.1016/j.epsl.2006.10.016.

Schulz, M., and M. Mudelsee (2002), REDFIT: Estimating red-noise spectra directly from unevenly spaced paleoclimatic time series, *Comput. Geosci.*, *28*(3), 421–426, doi:10.1016/S0098-3004(01)00044-9.

Shackleton, N. J. (1977), Carbon-13 in Uvigerina: Tropical rainforest history and the Equatorial Pacific carbonate dissolution cycles, in *The Fate of Fossil Fuel CO_2 in the Oceans New York*, edited by N. R. Andersen and A. Malahoff, pp. 401–427, Plenum Press, New York.

Siegenthaler, U., E. Monnin, K. Kawamura, R. Spahni, J. Schwander, B. Stauffer, T. F. Stocker, J. M. Barnola, and H. Fischer (2005), Supporting evidence from the EPICA Dronning Maud Land ice core for atmospheric CO_2 changes during the past millennium, *Tellus, Ser. B*, *57*(1), 51–57, doi:10.1111/j.1600-0889.2005.00131.x.

Sigman, D. M., and E. A. Boyle (2000), Glacial/interglacial variations in atmospheric carbon dioxide, *Nature*, *407*(6806), 859–869, doi:10.1038/35038000.

Tian, J., P. X. Wang, X. R. Cheng, and Q. Y. Li (2002), Astronomically tuned Plio-Pleistocene benthic $\delta^{18}O$ record from South China Sea and Atlantic-Pacific comparison, *Earth Planet Sci. Lett.*, *203*, 1015–1029, doi:10.1016/S0012-821X(02)00923-8.

Tian, J., D. K. Pak, P. X. Wang, D. Lea, X. R. Cheng, and Q. H. Zhao (2006), Late Pliocene monsoon linkage in the tropical South China Sea, *Earth Planet. Sci. Lett.*, *252*(1–2), 72–81, doi:10.1016/j.epsl.2006.09.028.

Tiedemann, R., M. Sarnthein, and N. J. Shackleton (1994), Astronomic timescale for the Pliocene Atlantic $\delta^{18}O$ and dust flux records of ocean drilling program site 659, *Paleoceanography*, *9*(4), 619–638, doi:10.1029/94PA00208.

Toggweiler, J. R. (1999), Variation of atmospheric CO_2 by ventilation of the ocean's deepest water, *Paleoceanography*, *14*(5), 571–588, doi:10.1029/1999PA900033.

Toggweiler, J. R. (2008), Origin of the 100,000-year timescale in Antarctic temperatures and atmospheric CO_2, *Paleoceanography*, *23*(2), PA2211, doi:10.1029/2006PA001405.

Vance, D., D. A. H. Teagle, and G. L. Foster (2009), Variable Quaternary chemical weathering fluxes and imbalances in marine geochemical budgets, *Nature*, *458*(7237), 493–496, doi:10.1038/nature07828.

Venz, K. A., and D. A. Hodell (2002), New evidence for changes in Plio-Pleistocene deep water circulation from Southern Ocean ODP Leg 177 Site 1090, *Palaeogeogr. Palaeoclimatol. Palaeoecol.*, *182*, 197–220, doi:10.1016/S0031-0182(01)00496-5.

Walker, J. C. G., P. B. Hays, and J. F. Kasting (1981), A negative feedback mechanism for the long-term stabilization of Earth's surface-temperature, *J. Geophys. Res.*, *86*(C10), 9776–9782, doi:10.1029/JC086iC10p09776.

Wang, P. X., J. Tian, X. R. Cheng, C. L. Liu, and J. Xu (2003), Carbon reservoir changes preceded major ice-sheet expansion at the mid-Brunhes event, *Geology*, *31*(3), 239–242, doi:10.1130/0091-7613(2003)031<0239:CRCPMI>2.0.CO;2.

Wang, P. X., J. Tian, X. R. Cheng, C. L. Liu, and J. Xu (2004), Major Pleistocene stages in a carbon perspective: The South China Sea record and its global comparison, *Paleoceanography*, *19*, PA4005, doi:10.1029/2003PA000991.

Woodruff, F., and S. Savin (1991), Mid-Miocene isotope stratigraphy in the deep sea: High-resolution correlations, Paleoclimatic cycles, and sediment preservation, *Paleoceanography*, *6*(6), 755–806, doi:10.1029/91PA02561.

Zeebe, R. E., and K. Caldeira (2008), Close mass balance of long-term carbon fluxes from ice-core CO_2 and ocean chemistry records, *Nat. Geosci.*, *1*(5), 312–315, doi:10.1038/ngeo185.

Zeebe, R. E., and P. Westbroek (2003), A simple model for the $CaCO_3$ saturation state of the ocean: The "Strangelove," the "Neritan," and the "Cretan" Ocean, *Geochem. Geophys. Geosyst.*, *4*(12), 1104, doi:10.1029/2003GC000538.

M. Elliot and T. Russon, Grant Institute of Earth Sciences, School of GeoSciences, University of Edinburgh, the Kings Buildings, Edinburgh EH9 3JW, UK. (t.f.russon@sms.ed.ac.uk)

D. Paillard, Laboratoire des Sciences du Climat et de l'Environnement, IPSL, CNRS, Orme des Merisiers, Bat. 701, Gif-sur-Yvette F-91191, France.